Advances in Modern Agriculture (2022) Volume 3 Issue 1
doi: 10.54517/ama.v3i1.2047

Asia Pacific Academy of Science Pte. Ltd.

ORIGINAL RESEARCH ARTICLE

Gradient throwing characteristics of oscillating slat shovel for rhizome crop harvesters

Lipengcheng Wan[1,2], Yonglei Li[1,2,*], Hu Zhao[1,2], Guanghao Xu[1,2], Jiannong Song[1,2], Xiangqian Dong[1,2], Chao Zhang[3], Jicheng Wang[1,2]

[1] *College of Engineering, China Agricultural University, Beijing 100083, China*

[2] *Key Laboratory of Soil-Machine-Plant System Technology, Ministry of Agriculture and Rural Affairs, Beijing 100083, China*

[3] *School of Mechatronics Engineering, Henan University of Science and Technology, Luoyang 471023, Henan Province, China*

*** Corresponding author:** Yonglei Li, liyl0393@cau.edu.cn

ABSTRACT

An oscillating slat shovel has presented a promising application potential in the energy-saving and efficient harvesting of deep rhizome crops. This new type of shovel slat integrated harvesting device was developed using gradient amplitude and gradient vibration technology. This study aims to clarify the working characteristics of oscillating slat shovels and the mechanism of throwing separation. The throwing coefficient was selected to characterize the throwing separation ability of the slat shovel work plane. A motion analysis was made to calculate the swing acceleration of the slat shovel work plane. An analytical equation of the throwing coefficient was then established to combine with the working process, the periodic variation of the throwing coefficient, and the influence of parameters, including the amplitude, vibration frequency, and working length. The results showed that the throwing coefficient gradually increased at each point of the slat shovel work plane, indicating outstanding gradient throwing characteristics and strong throwing ability. The maximum throwing coefficient was 9.98–19.72 in the separation area. After that, an investigation was made to determine the influence of the structure and working parameters of the oscillating slat shovel on the soil-throwing separation performance. The EDEM-MBD coupling simulation model of the single pendulum shovel gate was established to simplify the structural model and the interaction between the rhizome, soil, and working components, where the indicators were set as the traction resistance, driving torque, the maximum separation distance between the soil and the slat (separation distance), and the ratio of the separated soil quality of each functional area of the work-plane to the total soil mass (separation ratio). A single-factor test was carried out with the amplitude, vibration frequency, and forward speed as factors. The results indicated that: 1) There were outstanding strong-weak cycles in the traction resistance and driving torque due to the gradient throwing characteristics of the oscillating slat shovel, soil viscosity, and plasticity. In the strong period, there was a large interaction force between the shovel slat and soil, where the maximum separation distance occurred at the middle point of the separation area at the endpoint of the cutting stroke. 2) The amplitude was negatively correlated to the traction resistance but positively correlated with the driving torque and separation distance. The vibration frequency was negatively correlated to the traction resistance, driving torque, and separation spacing. The forward velocity was positively correlated to traction resistance and driving torque but negatively correlated to the

ARTICLE INFO
Received: 15 May 2022 | Accepted: 1 June 2022 | Available online: 26 June 2022

CITATION
Wan L, Li Y, Zhao H, et al. Gradient throwing characteristics of oscillating slat shovel for rhizome crop harvesters. *Advances in Modern Agriculture* 2022; 3(1): 2047. doi: 10.54517/ama.v3i1.2047

separation distance. 3) There was a small influence of amplitude and vibration frequency on the separation ratio. There was a low separation of oscillating slat shovels with the increase in forward velocity. 4) A combination of parameters was achieved when the amplitude was 7–11 mm in the strong period, where the average traction resistance was about 1580.93–2019.9 N, the maximum driving torque was about 224.04–322.11 N·m, and the maximum separation distance was about 59.58–98.3 mm. 5) The average traction resistance was about 1416.43–1866.38 N, the maximum driving torque was about 315.28–364.19 N·m, and the maximum separation distance was about 78.43–94.67 mm when the vibration frequency was 6.67–10.67 Hz. 6) The average traction resistance was about 1429.43–2110.48 N, the maximum driving torque was about 241.27–387.78 N·m, and the maximum separation distance was about 62.5–102.5 mm when the forward speed was 0.2–0.4 m/s. An optimal combination of parameters was selected for the field experiment: the amplitude was 9 mm, the vibration frequency was 9.4 Hz, and the working speed was 0.32 m/s. The licorice harvesting test indicated that the traction resistance was about 32.17 kN, the driving torque was about 802.02 N·m, the excavation depth was about 468 mm, and the cleaning rate was about 96.42%. Consequently, the oscillating slat shovel harvesting device can be feasible for smooth and orderly operation as well as the higher separation performance of rhizome-soil, where all the operation indexes meet the national standards. This finding can provide a new method and design reference for the energy-saving and efficient harvesting of rhizomes, especially deep rhizome crops.

Keywords: harvest; simulation; rhizome; oscillating slat shovel; gradient throwing

1. Introduction

Potatoes, peanuts, cassava, licorice, and rhizome crops, such as Panax, are important cash crops, and mechanized harvesting is the weak link in the whole mechanized production of root crops (2019 machine harvesting rate: about 26% for potatoes, 50% for peanuts, and 14.6% for root herbs), which seriously restricts the development of related industries[1–4]. Rootstock crop harvesting mainly refers to the comprehensive operational process of digging underground rootstocks (fruits) from the soil and achieving effective separation of rootstocks from the soil. The existing harvesting equipment at home and abroad mainly adopts the structure form of "excavation device + transport separation device", including shovel and sieve integrated type, shovel and sieve combination type, shovel chain combination type, shovel roller combination type, and other typical structures[5–9]. Because the excavation and separation processes involve a large amount of soil work, especially when the excavation depth is deep and the mixture separation volume is large, the contradiction between the harvesting efficiency and the energy consumption of the machine is prominent[10–13].

Focusing on the demand for energy-saving harvesting of root crops with reduced resistance, relevant scholars at home and abroad have carried out a lot of research work on structural innovation of harvesting devices and efficient separation of root and soil. Yang et al.[14] designed a paddle roller push potato harvester and studied the operating mechanism of the push conveyor separation device; Hou et al.[15] designed a self-propelled onion combine harvester by combining onion planting patterns and agronomic systems; Yang et al.[16] designed a self-propelled cassava harvester with a lifting chain soil-potato separation device by integrating the processes of cassava excavation, clamping and conveying, potato-stem separation, and soil removal and collection; Lv et al.[17] designed a self-propelled cassava harvester by optimizing the lifting chain soil separation device. Lv et al.[17] optimized the structure design of the lifting chain and shaker to enhance the separation of the potato-soil mixture; Xie et al.[18] analyzed the structure and operating parameters affecting the operating performance of the swing separating the screen and obtained the optimized parameter combination; Wei et al.[19] obtained the structure and operating parameters of the wavy screen surface of the potato harvester based on discrete element simulation analysis.

The single pendulum shovel fence is a light and simple energy-saving harvesting device developed by the author's team based on the technological innovation of crank rocker mechanism rocker amplitude and

directional vibration. Previous experimental studies on cassava, licorice, and other root crop harvesting have shown that the monoshaker grate harvesting device has low vibration cutting resistance, low ineffective energy consumption for soil transport, high efficiency for vertical separation of materials during harvesting, and good potential for application in root crops, especially deep root crops harvesting[20–23], but the working characteristics of the monoshaker grate are not clear, and the mechanism of energy-saving operation is not clear, which restricts its technical maturation and However, the working characteristics of a single-swing fence are not clear, and the mechanism of energy-saving operation is not clear.

In order to clarify the working characteristics of the monopod grate and investigate the influence of the working parameters on its throwing and separating ability, this paper establishes the analytical equations of the throwing coefficients on the working surface of the grate based on kinematics and dynamics analysis to characterize the asymptotic throwing characteristics and throwing and separating ability of the monopod grate. The single-factor simulation test was carried out with traction resistance (F), driving torque (T), separation distance (H), and separation ratio (C) as indicators, in order to obtain the action law and influence mechanism of working parameters such as amplitude (A), vibration frequency (f), and forward speed (V).

2. Single pendulum shovel fence harvesting device structure and working principle

2.1. General structure

The device is mainly composed of a transmission system, an excitation device, an excavation separation device, a frame, etc. The transmission system includes a variable speed gearbox, transmission shaft, coupling, etc.; the excitation device includes an eccentric shaft, connecting rod, pendulum, mounting bearing seat, etc., divided into three groups of left, middle, and right (eccentric shaft crank installation phase angle staggered 180° in turn); the excavation separation device includes a shovel frame, excavation shovel, separation fence, etc., divided into three groups of the left shovel, middle shovel, and right shovel. The overall structure is shown in **Figure 1**.

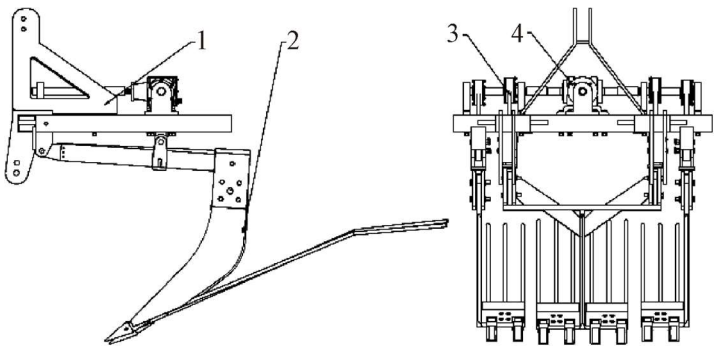

Figure 1. Structure diagram of oscillating slat shovel harvest device.
Note: 1. Frame; 2. Excavation and separation device; 3. Vibration device; 4. Driving system.

2.2. Working principle

During the harvesting operation, the tractor power output shaft power through the traditional system is distributed to the left, middle, and right three groups of excitation devices, installed in the excitation device pendulum on the excavation and separation device alternately cutting excavation soil and throwing the separation of root-soil mixture, broken and scattered soil through the gap of the fence into the excavation and separation device below, and the root via the fence slides on the surface after the operation.

The structure of the device can be simplified as a crank rocker mechanism, with the pendulum (i.e., rocker) swinging around the pendulum pin point cycle, digging separation device work surface points due to the different radius of swing and having different swing amplitude, vibration direction angle, and motion trajectory, as shown in **Figure 2**.

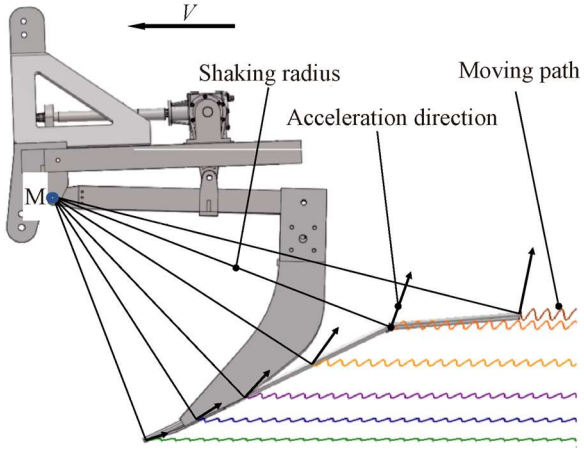

Figure 2. Movement diagram of oscillating slat shovel.
Note: M is the joint of the pendulum pin; V is working speed, m·s^{-1}.

3. Key components

3.1. Excitation device

The device is mainly composed of gearbox, eccentric shaft, connecting rod, pendulum, etc., as shown in **Figure 3**. The gearbox output speed can be converted into the swing frequency (vibration frequency f) of the pendulum, and the eccentric distance (amplitude A) of the eccentric shaft (crank) can be converted into the pendulum and the unequal working pendulum at each point of the working surface.

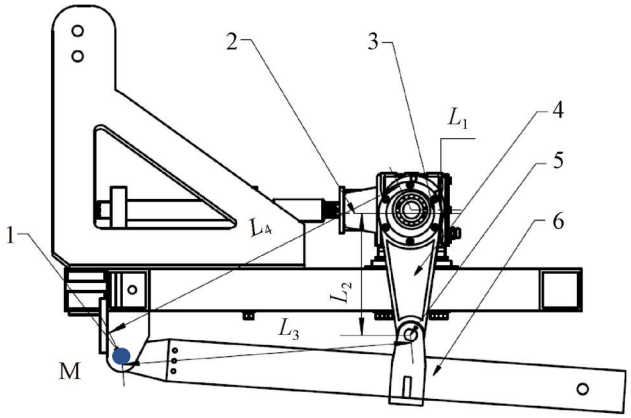

Figure 3. Structure diagram of excitation device.
Note: L_1 is eccentricity, mm; L_2 is the length of the connecting rod, mm; L_3 is the length of the pendulum rod, mm; L_4 is the distance between the eccentric shaft and pendulum pin shaft, mm. 1. Pendulum pin; 2. Gearbox; 3. Eccentric shaft; 4. Connecting rod; 5. Connecting rod pin 6. Pendulum rod.

Based on the previous study, the structural parameters of the single pendulum shovel grid were determined to be L_1 of 9 mm, L_2 of 260 mm, L_3 of 534.6 mm, and L_4 of 628.7 mm, with the main operating parameters ranging from A to 11 mm, f of 6.67 to 10.67 Hz, and V of 0.2 to 0.4 m/s.

3.2. Excavation separation device

The device mainly includes the left shovel, middle shovel, and right shovel, as shown in **Figure 4**. The digging shovel is made of 65Mn steel plate and several digging teeth (WGXS60C-1); the separation fence is made of φ20 mm round steel bent and welded on the shovel frame; the fence spacing is usually 80–120 mm according to the shape size of the harvested object and soil separation volume; and the fence spacing is 100 mm according to the pre-test of licorice harvesting. The working surface is divided into digging and loosening zones (digging zone, *W* zone), winnowing and dispersing zones (dispersing zone, *B* zone), and shaking and separating zones (separating zone, *D* zone).

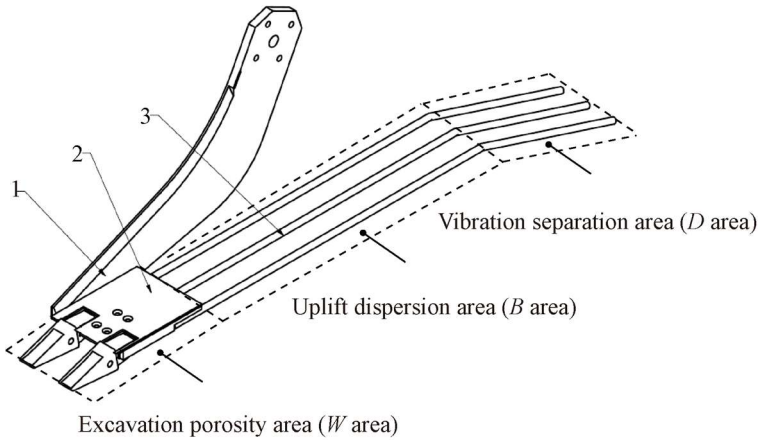

Figure 4. Structure diagram of excavation separation device.
Note: 1. Shovel rack; 2. Excavation shovel; 3. Separation slat.

The necessary conditions for the normal operation of the excavation and separation device are that the excavation shovel should have a reasonable shovel face inclination to achieve smooth soil entry and excavation, and the working surface should have sufficient working length and the end of the separation fence should be slightly higher than the ground surface by 50–100 mm. The sketch of the working surface structure of the shovel fence is shown in **Figure 5**. The working length is composed of three parts: the excavation length l_W, the dispersion length l_B, and the separation length l_D. According to the preliminary experimental research and reference to the existing root harvesting equipment, the shovel face inclination angle α_{W0} = 25°, l_W =480 mm; excavation depth h = 500 mm, dispersion zone fence inclination angle α_{B0} = 25°; separation length l_D = 495 mm, fence tail height h_1 = 60 mm, separation zone fence inclination angle α_{D0} = 7°; dispersion length $l_B = \frac{h}{sin\alpha_W} - l_W = 703\ mm$, working length $l = l_W + l_B + l_D$ = 1678 mm.

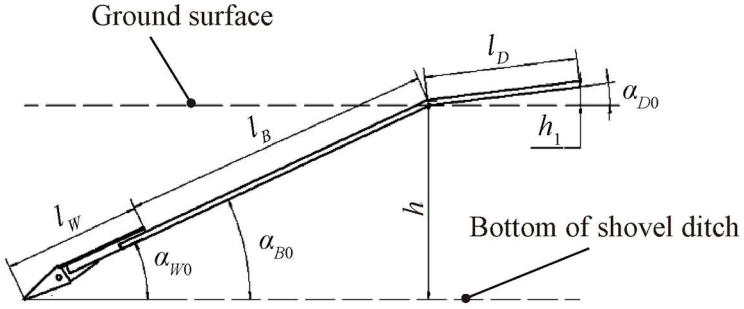

Figure 5. Structural diagram of slat shovel work-plane.
Note: l_W is excavation length, mm; l_B is dispersion length, mm; l_D is separation length, mm; α_{W0} is inclination angle of shovel surface, (°); α_{B0} is inclination angle of slat surface in the dispersion area, (°); α_{D0} is inclination angle of slat surface in separation area, (°); h is the working depth, mm; h_1 is the height of separation end point, mm.

4. Analysis of the operating characteristics of the single pendulum shovel grid

The throwing coefficient is used to characterize the throwing separation capacity of the working surface of the shovel fence, and the formula for calculating the oscillation acceleration of the working surface of the shovel fence is obtained through motion analysis.

4.1. Single pendulum shovel grid motion analysis

The motion analysis of the single pendulum is shown in **Figure 6**. L_1 is 9 mm, L_2 is 260 mm, L_3 is 534.6 mm, L_4 is 628.7 mm, and the pendulum pin point M is the origin with the coordinates of point A (530, 326). Any point on the work surface is marked as E_{ij}, where i indicates the functional area, the values are W, B, D, and the starting and ending points of each area are marked as E_{i0}, E_{in}. E_{W0} coordinates (648, –704), the crank angle $\theta_{10} = 333.72^\circ$ and the pendulum angle $\theta_{30} = 6.53^\circ$.

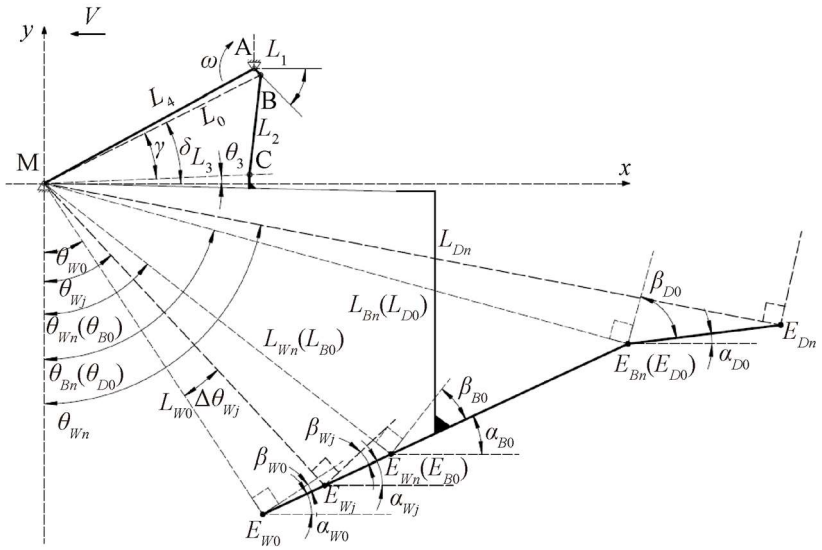

Figure 6. Motion analysis diagram of oscillating slat shovel.

Note: A is the rotation center of crank; B is the joint of crank and connecting rod; C is the joint of connecting rod pin; L_0 is the distance between B and M, mm; Δ is the angle between BM and x axis, (°); γ is the angle between BM and CM, (°); θ_1 is the angle of crank (between crank and x axis, initial value is θ_{10}), $\theta_1 = \omega t$, (°); θ_3 is the angle of pendulum (between pendulum and x axis, initial value is θ_{30}), (°); ω is the angular velocity of crank, rad·s^{-1}; E_{ij} is one point of work-plane; E_{W0} is shovel tip (start point of excavation area); $E_{Wn}(E_{B0})$ is the end point of excavation area (start point of the dispersion area); $E_{Bn}(E_{D0})$ is the end point of the dispersion area (start point of separation area); E_{Dn} is the end point of the separation area; L_{ij} is swing radius of E_{ij}, mm; θ_{ij} is the angle between swing radius of E_{ij} and y axis (initial value is θ_{ij0}), (°); $\Delta\theta_{Wj}$ is angle variation between excavation area swing radius and y axis; α_{ij} is the angle between E_{ij} and x axis, (°) (initial value is $\theta_{ij0}, i = W, B, D; j = 0,1,2,3 \ldots$); β_{ij} is the angle between vibration direction angle of E_{ij} and work-plane, (°) (initial value is β_{ij} , $i = W, B, D; j = 0,1,2,3 \ldots$).

4.1.1. Pendulum swing angle and angular acceleration

Point A is labeled as $(x_\mathrm{A}, y_\mathrm{A})$, point M is labeled as $(x_\mathrm{M}, y_\mathrm{M})$,then the system of equations for the position of point B is as follows (Equation (1)).

$$\begin{cases} x_\mathrm{B} = x_\mathrm{A} + L_1 \cos\theta_1 \\ y_\mathrm{B} = y_\mathrm{A} - L_1 \sin\theta_1 \end{cases} \tag{1}$$

The angle δ between BM and x-axis is calculated by Equation (2).

$$\delta = \tan^{-1}\left(\frac{y_\mathrm{B} - y_\mathrm{M}}{x_\mathrm{B} - x_\mathrm{M}}\right) \tag{2}$$

According to the derivation of the cosine theorem, the angle γ between BM and CM is calculated by Equation (3).

$$\gamma = \cos^{-1}(\frac{L_0^2 + L_3^2 - L_2^2}{2L_0L_3}) \tag{3}$$

The CM pendulum angle θ_3 is calculated by Equation (4).

$$\theta_3 = \delta - \gamma \tag{4}$$

CM pendulum angle θ_3 variation $\Delta\theta_3 = \theta_3 - \theta_{30}$; CM angular acceleration ε_3 calculated by Equation (5).

$$\varepsilon_3 = \frac{\mathrm{d}^2 + \theta_3}{\mathrm{d}t^2} \tag{5}$$

Applying MATLAB software to compile Equations (1)–(5), when the amplitude A is 9 mm and the vibration frequency f is 8.67 Hz, θ_3 and ε_3 show a sinusoidal period variation with θ_3 values of 0.1069° to 0.1408° and ε_3 values of –48 to 52 rad/s^2. The periodic variation curves of θ_3 and ε_3 are shown in **Figure 7**.

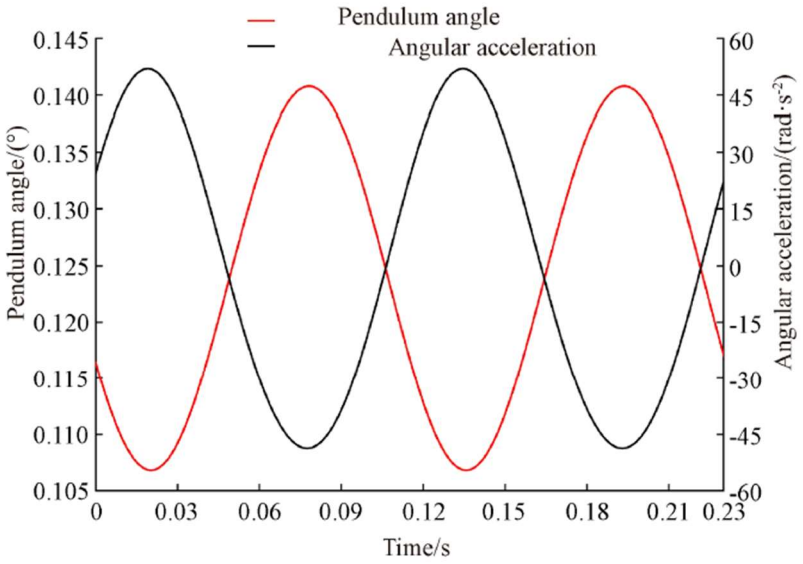

Figure 7. Periodic variation curve of pendulum angle and angular acceleration.

4.1.2. Shovel grate inclination angle, vibration direction angle, swing acceleration

The working surface can be simplified as a fold line consisting of three straight line segments. The coordinates of the position of point E_{ij} at the initial moment t_0 can be expressed by Equation (6).

$$y_{ij} = \begin{cases} 0.466x_{Wj} - 1005.97, x_{Wj} \in [648,850] \\ 0.466x_{Bj} - 1005.97, x_{Bj} \in [850,1720] \\ 0.123x_{Dj} - 415.96, x_{Dj} \in [1720,2212] \end{cases} \tag{6}$$

1) Shovel grate inclination angle

E_{ij} Point fence inclination $\alpha_{ij} = \alpha_{ij} + \Delta\theta_3$, fence inclination in the digging area $\alpha_{Wj} = \alpha_{Wj} + \Delta\theta_3$, $\alpha_{Wj} = \alpha_{W0} = 25°$; fence inclination in the dispersion area $\alpha_{Bj} = \alpha_{Bj} + \Delta\theta_3$, $\alpha_{Bj} = \alpha_{B0} = 25°$; fence inclination in the dispersion area $\alpha_{Dj} = \alpha_{Dj} + \Delta\theta_3, \alpha_{Dj} = \alpha_{D0} = 7°$.

2) Vibration direction angle

The coordinates of the starting point E_{i0} position of each zone are calculated from Equation (7).

$$\begin{cases} x_{i0} = x_{\mathrm{M}} + L_{i0}\sin\theta_{i0} \\ y_{i0} = y_{\mathrm{M}} - L_{i0}\cos\theta_{i0} \end{cases} \tag{7}$$

where $\theta_{i0} = \theta_{i0} + \Delta\theta_3$, θ_{i0} is the starting pendulum angle of each zone, (°); θ_{i0} is the initial pendulum angle of each zone, (°).

The coordinates of the position of an arbitrary point E_{ij} are calculated by Equation (8):

$$y_{ij} = \tan\alpha_{ij}\left(x_{ij} - x_{i0}\right) + y_{i0} \tag{8}$$

where $x_{ij} \in [x_{i0}, x_{in}]$, mm.

The length of $L_{E_{i0}E_{ij}}$ the line segment E_{i0} – E_{ij} is calculated from Equation (9):

$$L_{E_{i0}E_{ij}} = \sqrt{\left(x_{ij} - x_{i0}\right)^2 + \left(y_{ij} - y_{i0}\right)^2} \tag{9}$$

The radius of oscillation L_{ij} of the point E_{ij} is calculated by Equation (10):

$$L_{ij} = \sqrt{L_{i0}^2 + L_{E_{i0}E_{ij}}^2 - 2L_{i0}L_{E_{i0}E_{ij}} \cdot \cos\left(\frac{\pi}{2} + \beta_{i00}\right)} \tag{10}$$

where β_{i00} is the initial vibration direction angle at point E_{i0}, (°).

$\Delta\theta_{ij}$ is the angle between the pendulum L_{i0} and L_{ij} calculated by Equation (11):

$$\Delta\theta_{ij} = \cos^{-1}\left(\frac{L_{i0}^2 + L_{ij}^2 - L_{E_{i0}E_{ij}}^2}{2L_{i0}L_{ij}}\right) \tag{11}$$

where $\Delta\theta_{ij}$ is the angle between the E_{ij} point swing radius L_{ij} and the *y*-axis, and $\theta_{ij} = \theta_{ij0} + \Delta\theta_3$, (°).

The vibration direction angle β_{ij} is calculated from Equation (12):

$$\beta_{ij} = \theta_{ij} - \alpha_{ij} \tag{12}$$

where α_{ij} is the inclination angle of the shovel grate, (°).

3) Oscillation acceleration

According to E_{ij} the parameter values in section 3.1, when *f* is 6.67–10.67 Hz, the tangential acceleration $a_{\mathrm{t}_{ij}}$ at any point on the working surface is much greater than the normal acceleration $a_{\mathrm{n}_{ij}}$, and the oscillation acceleration a_{ij} at that point is simplified to the tangential acceleration $a_{\mathrm{t}_{ij}}$, which is calculated by Equation (13).

$$a_{ij} = a_{\mathrm{t}_{ij}} = L_{ij}\varepsilon_3 \tag{13}$$

4.2. Single pendulum shovel fence operation process analysis

4.2.1. Trajectory of shovel tip movement

Each point of the working surface of the shovel fence has a similar motion law, take the shovel tip as an example to analyze the operation process of a single pendulum shovel fence, and apply the kinematic simulation module of RecurDyn V9R2 software to draw the trajectory of the shovel tip E_{W0} point, as shown in **Figure 8**. During the cutting process (J_0~J_1 section), the excavation area is the main working area, the shovel tip drops from the highest point to the lowest point, and the cut soil is forced to slip and lift along the working face; during the lifting and throwing process (J_1~J_2 section), the dispersion area and separation area are the

main working areas, the tip of the shovel rises from the lowest point to the highest point, the soil collides with the grid and disperses and falls below the grid, and the rhizomes are caught above the grid and move backwards, realizing rhizome soil separation.

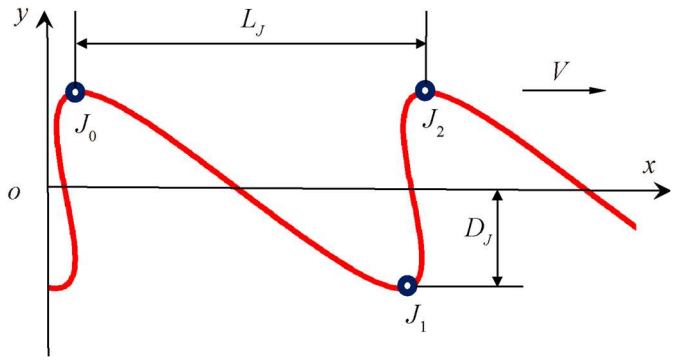

Figure 8. Trajectory of shovel tip.
Note: J_0, J_2 is starting point of cutting stroke; J_1 is starting point of lifting stroke; L_J is Periodic horizontal displacement of shovel tip; D_J is working amplitude for shovel tip, mm.

4.2.2. Soil particle forces on the working surface of the shovel grid

To simplify the calculation, the soil particle at the point E_{ij} is simplified as a mass point, which is subjected to the combined action of gravity G_{ij}, support force F_{Nij}, front soil resistance F_{ij}, frictional resistance f_{ij}, inertia force F_{aji}, etc., as shown in **Figure 9**.

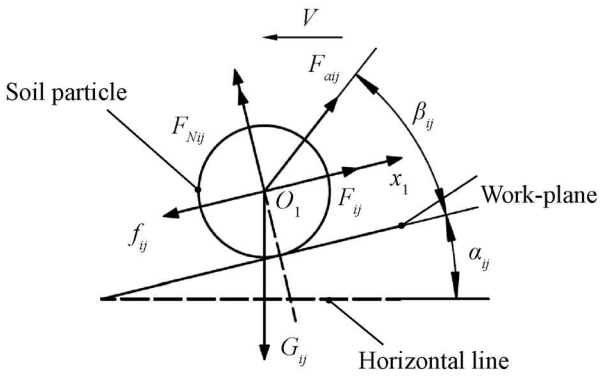

Figure 9. Force analysis of soil particles.
Note: α_{ij} is the inclination angle of slat shovel, (°); β_{ij} is the vibration direction angle, (°); G_{ij} is the gravity, N; F_{Nij} is the supporting force, N; F_{ij} is the front soil resistance, N; f_{ij} is the frictional resistance, N; F_{aij} is the inertial force, N.

As shown in Equation (14), support F_{Nij} for

$$F_{\mathrm{N}ij} = F_{aij}\sin\beta_{ij} - G_{ij}\cos\alpha_{ij} \tag{14}$$

When $F_{Nij} \leq 0$, the soil particles at the point E_{ij} are thrown up, then there is Equation (15):

$$F_{\mathrm{N}ij} = F_{aij}\sin\beta_{ij} - G_{ij}\cos\alpha_{ij} \leq 0 \tag{15}$$

E_{ij} The point vibration intensity K_{ij} can be expressed as Equation (16):

$$K_{ij} = \frac{a_{ij}}{g} = \frac{L_{ij}\varepsilon_3}{g} \tag{16}$$

The throwing coefficient K_{Vij} is used to characterize the throwing and separating ability of the working surface of a single pendulum shovel grid. K_{Vi} is defined as the difference between the normal upward swinging

acceleration component of the working surface and the ratio of the gravitational acceleration components is shown in Equation (17):

$$K_{Vij} = \frac{a_{ij}\sin\beta_{ij}}{g\cos\alpha_{ij}} = \frac{L_{ij}\varepsilon_3\sin\beta_{ij}}{g\cos\alpha_{ij}} \tag{17}$$

4.3. Gradual throwing characteristics of shovel fence working surface

4.3.1. Variation law of throwing coefficient

According to the parameter values in section 3.1, *V* is selected as 0.3 m/s, vibration frequency *f* is 8.67 Hz, amplitude *A* is 9 mm, and the midpoint of each area of the shovel grid working surface is taken as the characteristic point, and the relevant parameters are substituted into Equation (17) to obtain the throwing coefficients of each point analytically, as shown in **Figure 10**.

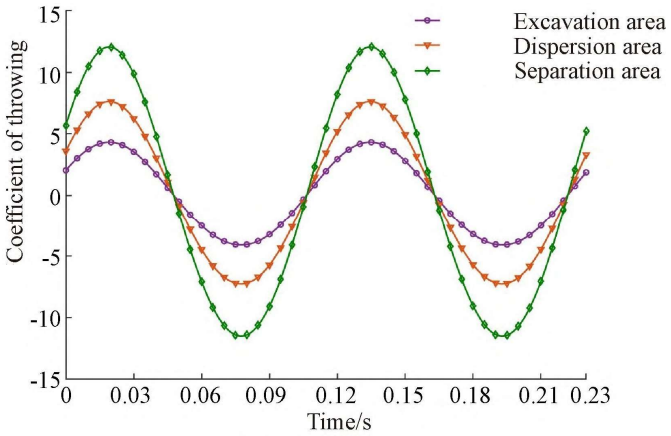

Figure 10. Variation curve of throwing coefficient.

The mid-point throwing coefficient of each zone varies sinusoidally and increases with the increase of the swing radius, when $K_{Vij} > 0$ can effectively throw the soil; the maximum throwing coefficient of each zone is the maximum throwing coefficient of the mid-point of the dispersal zone $K_{VBMmax} = 1.73K_{VWMmax}$, the maximum throwing coefficient of the mid-point of the separation zone $K_{VBMmax} = 2.74K_{VWMmax}$. K_{VWMmax} is the maximum throwing coefficient in the excavation zone.

4.3.2. Analysis of the asymptotic law of the throwing coefficient

The maximum throwing coefficient at each point of the working surface is used as an index to analyze the effect of amplitude-working length and vibration frequency-working length interaction.

1) Amplitude—working length impact analysis

According to the values of parameters in section 3.1, when V is 0.3 m/s and f is 8.67 Hz, the amplitudes A are taken as 7, 8, 9, 10 and 11 mm, respectively, and the relevant parameters are substituted into Equation (17) to obtain the maximum throwing coefficients K_{Vijmax} at each point of the working surface analytically, as shown in **Figure 11**.

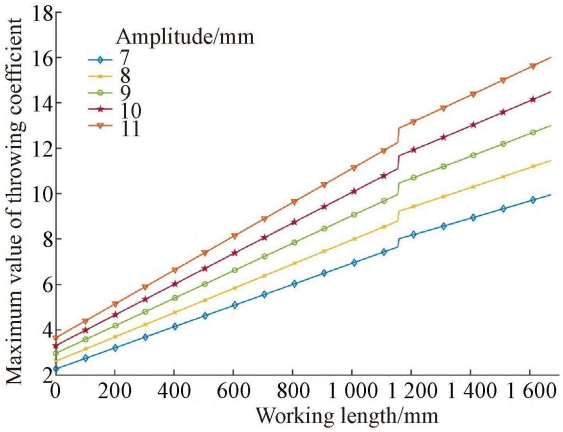

Figure 11. Relation graph of amplitude, working length and maximum value of throwing coefficient.

The maximum throwing coefficient K_{Vijmax} increases with the increase of working length and $K_{Vijmax} > 2$, all zones of the working surface can throw the soil effectively, the maximum throwing coefficient of excavation zone K_{VW} is 4.50–7.46, the maximum throwing coefficient of dispersal zone K_{VBmax} is 7.58–12.24, the maximum throwing coefficient of separation zone K_{VDmax} is 9.98–16.02, which has a strong shaking separation effect.

The maximum throwing coefficient increases with the increase of amplitude A. When A=11 mm, the maximum throwing coefficients of each area of the working surface are $K_{VWmax} = 7.46$, $K_{VWmax} = 12.24$ and $K_{VWmax} = 16.02$, respectively.

2) Vibration frequency-working length influence analysis

According to the values of parameters in section 3.1, when V is 0.3 m/s and A is 9 mm, the vibration frequencies f are taken as 6.67, 7.67, 8.67, 9.67, and 10.67 Hz, respectively, and the maximum throwing coefficient at each point of the working surface is obtained analytically K_{Vijmax}, as shown in **Figure 12**.

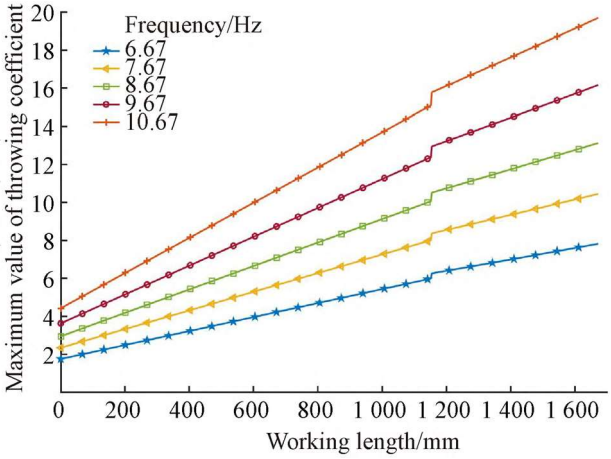

Figure 12. Relation graph of frequency, working length and maximum value of throwing coefficient.

The maximum throwing coefficient increases with the increase of working length; the maximum throwing coefficient in the excavation zone K_{VWmax} is 3.52–8.74, the maximum throwing coefficient in the dispersion zone K_{VBmax} is 6.02–15.4, and the maximum throwing coefficient in the separation zone K_{VDmax} is 7.83–19.72. The throwing coefficients in each zone have a wide range of variation.

The maximum throwing coefficient increases with the increase of vibration frequency, and when f = 10.67 Hz, the maximum throwing coefficients of each zone are $K_{VWmax} = 8.74$, $K_{VBmax} = 15.4$, and K_{VDmax}=19.72 respectively.

5. Simulation analysis of single pendulum shovel grid throwing separation performance

In order to clarify the influence law of the structure and working parameters of the monopod grate on the soil throwing and separation performance, a monopod grate virtual soil tank EDEM-MBD coupling simulation model was established by simplifying the structural model and the rootstock-soil-working part interaction relationship (without considering the influence of rootstock for the time being)[24–27] to carry out simulation experiments.

5.1. Simulation model construction and target data acquisition

5.1.1. EDEM-MBD coupled simulation model

The virtual soil tank (4000 mm × 280 mm × 1000 mm, soil thickness of 550 mm, total 287,000 particles) was established by using the EEPA contact model in EDEM2020 software; the simplified single pendulum shovel grid 3D model was constructed by Inventor software, and the MBD model was established by importing it into RecurDyn V9R2 software; the right shovel was imported into EDEM to establish the EDEM-MBD coupled simulation model, as shown in **Figure 13**.

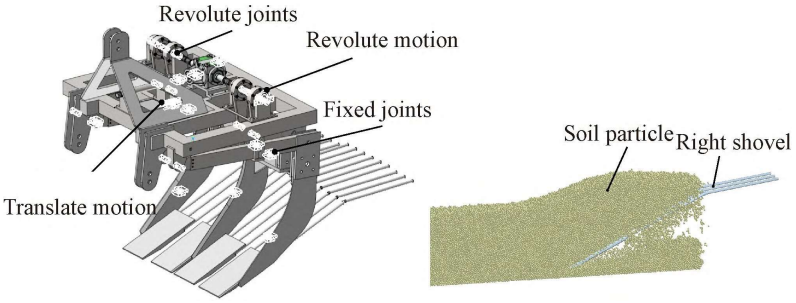

Figure 13. Simulation model of oscillating slat shovel.

The virtual soil tank intrinsic parameters and model parameters were set as[28–31]: soil particle size 13 mm, density 2160 kg/m^3, Poisson's ratio 0.26, and shear modulus 0.96 GPa, and the density of shovel grid material was 7865 kg/m^3, Poisson's ratio 0.3, and shear modulus 79 GPa, etc. The contact parameters of the EEPA contact model are shown in **Table 1**.

Table 1. Simulation model parameter table.

Parameter	Value
Collision recovery coefficient between soil particles	0.27
Statis friction coefficient between soil particles	0.57
Rolling friction coefficient between soil particles	0.32
Adhesion energy between soil particles/(J m^{-2})	26.30
Plastic deformation ratio between soil particles	0.41
Bonding branch index between soil particles	4.00
Tangential stiffness factor between soil particles	0.39
Collision recovery coefficient between soil particle and slat shovel	0.50
Statis friction coefficient between soil particle and slat shovel	0.30
Rolling friction coefficient between soil particle and slat shovel	0.10

5.1.2. Target data acquisition

Simulation test indexes of traction resistance, drive torque, separation spacing, and separation percentage were obtained using the following methods.

Traction resistance (*F*): The EDEM software post-processing interface extracts the resistance value of the working surface along the forward direction.

Driving torque (*T*): Recurdyn software Plot interface extracts the value of Driving torque in Torque motion.

Separation distance (*H*): In the post-processing of EDEM2020 software, the Clipping command is used to create the profile view of the monopendulum shovel fence-virtual soil groove at the end of the cutting stroke, and the image processing program is built in Python environment based on Opencv library. The separation spacing between the starting point, midpoint and end point of each area of the working surface is obtained by pixel point extraction and distance conversion, as shown in **Figure 14**.

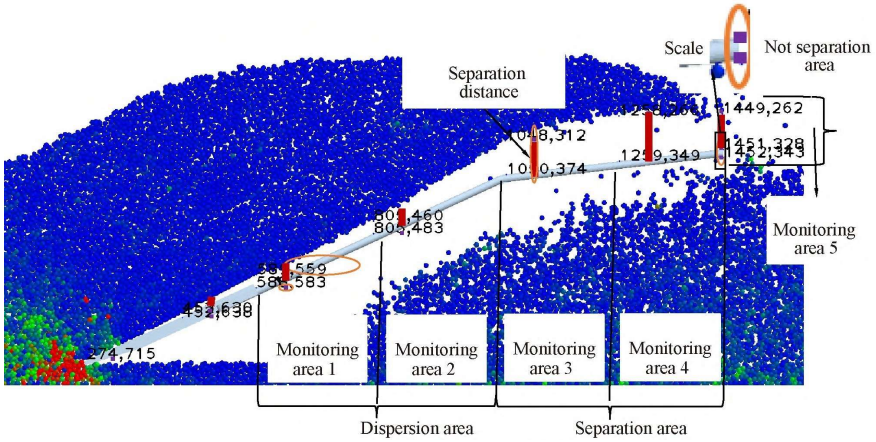

Figure 14. Obtained diagram of separation distance and separation ratio data.

Separation ratio (*C*): Five quality monitoring areas were set up in the dispersed area, separated area and unseparated area, and the EDEM post-processing follow-on quality monitoring sensors were used to obtain the average soil quality values of the monitoring areas, which were recorded as Q_1, Q_2, Q_3, Q_4 and Q_5, as shown in **Figure 14**. The ratio of separated soil mass (Q_k) to total soil mass C_k *in* each zone was calculated using Equation (18).

$$C_k = \frac{Q_k}{\sum_{k=1}^{5} Q_k} \times 100\% \tag{18}$$

5.1.3. Single pendulum shovel fence and soil interaction cycle analysis

According to the values of parameters taken in section 3.1, the trajectory of shovel tip movement and soil cycle force analysis for *A* of 9 mm, *f* of 8.67 Hz and *V* of 0.3 m/s are shown in **Figure 15**. The images at points 7, 8 and 9 in the figure have a significantly larger red area than the images at points 2, 3 and 4, indicating that the soil is subjected to a larger force at that moment.

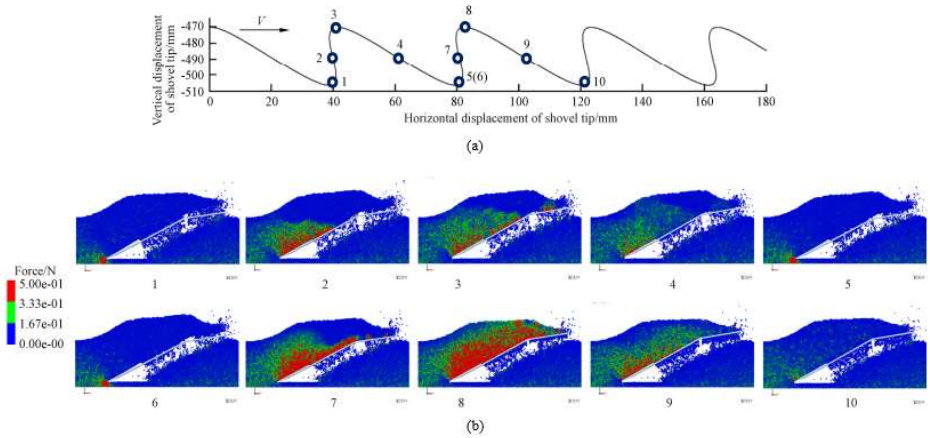

Figure 15. Analysis of shovel trajectory and soil force, **(a)**. Trajectory of shovel tip; **(b)**. Soil force at each job position of slat shovel. Note: 1 is lowest point, 2 is midpoint of lifting stroke, 3 is peak, 4 is midpoint of cutting stroke, 5 is lowest point, 6 is nadir, 7 is midpoint of lifting stroke, 8 is peak, 9 is midpoint of cutting stroke, 10 is nadir.

In the two adjacent cycles, the soil forces in both cutting and lifting strokes showed strong and weak cycles, especially in lifting strokes. The cycle with less soil stress (1–5 points) is called weak cycle (A_T cycle) and the cycle with more soil stress (6–10 points) is called strong cycle (B_T cycle), and the duration of each cycle is $T_a = T_b = \frac{1}{f}$.

5.2. The effect of amplitude on operational performance

According to the parameter taking values in section 3.1, the parameters V is 0.3 m/s, f is 8.67 Hz, digging depth is 500 mm, and A is 7, 9 and 11 mm, and the single-factor test is designed to clarify the effect of amplitude on operational performance.

5.2.1. Effect of amplitude on traction resistance and driving torque

The test results are shown in **Figure 16**. There are obvious strong and weak cycle phenomena of traction resistance $\bar{F}$ and driving torque T increase, A is negatively correlated with $\bar{F}$ and A is positively correlated with T. When A is 7, 9, 11 mm, the average values of traction resistance $\bar{F}$ in A_T cycle are 1376, 928.7, 696.8 N, and the maximum values of driving torque T_{max} are 103.16, 109.11, 141.28 N·m respectively. The mean values of traction resistance $\bar{F}$ during the B_T cycle were 2019.9, 1765.03, 1580.93 N; the maximum values of driving torque T_{max} were 224.04, 294.48, 322.11 N·m. When A increases from 7 mm to 9 mm, there is a large change in $\bar{F}$ in both A_T and B_T cycles, and T_{max} has a small increment in A_T cycle and a large increment in B_T cycle; when A increases from 9 mm to 11 mm, there is a small change in $\bar{F}$ in both A_T and B_T cycles, and T_{max} has a large increment in A_T cycle and a small increment in B_T cycle. Comprehensive analysis shows that the changes of $\bar{F}$ and T_{max} are relatively stable when A increases from 9 mm to 11 mm.

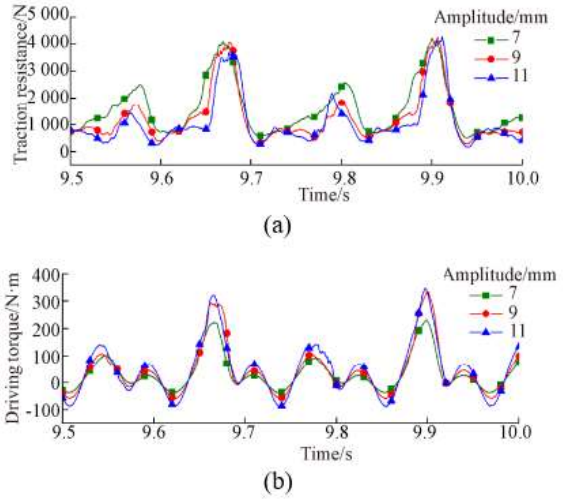

Figure 16. Effects of amplitude on traction resistance and driving torque, **(a).** Effects of amplitude on traction resistance; **(b).** Effects of amplitude on driving torque.

5.2.2. Effect of amplitude on throwing ability

The separation distance H at each point of the working surface is used to characterize the throwing ability of the single pendulum shovel fence, and a total of 7 characteristic points $E_{W0}, E_{WM}, E_{Wn}(E_{B0})$, $E_{BM}, E_{Bn}(E_{D0}), E_{DM}, E_{Dn}$ such as the starting point, the middle point and the ending point of each zone are selected from the analysis of the simulation results, it can be seen that the separation distance is relatively small during the A_T cycle, and the maximum value of the separation distance occurs at the end of the cutting stroke of the strong cycle (B_T), and the separation distance H at each point of the working surface when A is 7, 9 and 11 mm is obtained according to the method in section 5.1.2.

As can be seen from **Figure 17**, the separation spacing H is positively correlated with the amplitude A. The maximum value of the separation spacing H_{max} occurs at the middle point of the separation zone E_{DM} (affected by the soil viscoplasticity, the soil at the termination point of the separation zone E_{Dn} has fallen back to a certain height from the highest point). When A was 7, 9 and 11 mm, H_{max} was 59.58, 84.62 and 98.30 mm, respectively. During the B_T cycle, when A increased from 7 mm to 9 mm, H_{max} had a larger change.

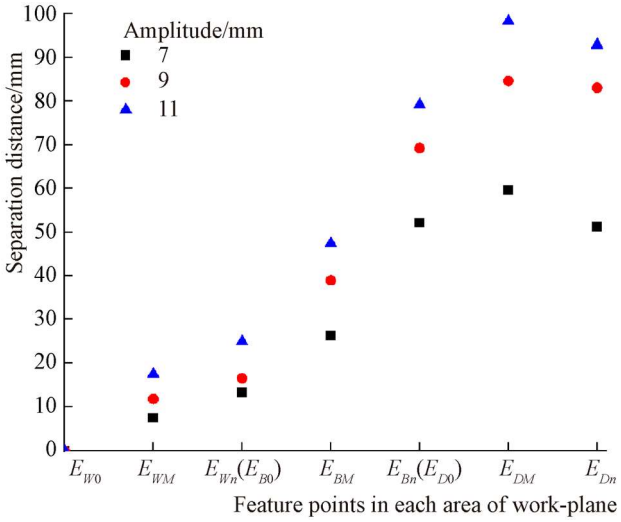

Figure 17. Effects of amplitude on separation distance.

Note: E_{WO} is starting point of excavation area, E_{WM} is midpoint of excavation area, $E_{Wn}(E_{B0})$ is ending point of excavation area (starting point of uplift dispersion area), E_{BM} is midpoint of dispersion area, $E_{Bn}(E_{D0})$ is ending point of dispersion area (starting point of vibration separation area), E_{DM} is midpoint of separation area, E_{Dn} is ending point of separation area.

5.2.3. Effect of amplitude on separation capacity

The soil quality of each quality monitoring area of the working face within 2.5 s of stable operation duration was counted, and the separation percentage C of each area of the working face when A was 7, 9, and 11 mm was obtained according to the method in section 5.1.2. as shown in **Table 2**.

Table 2. Separation proportion in each working area under different amplitudes(%).

Amplitude/mm	Monitoring area 1, 2 C_1+ C_2	Monitoring area 3, 4 C_3+ C_4	Monitoring area 5 C_5
7	64.35	30.26	5.39
9	64.59	31.00	4.41
11	64.85	32.39	2.76

From the analysis in **Table 2**, it can be seen that when A is 7, 9, and 11 mm, the overall change of separation ratio $C_1 + C_2$ in the dispersion zone and separation ratio $C_3 + C_4$ in the separation zone is not obvious, and the effect of amplitude A on the separation ratio C is less influenced by soil viscoplasticity.

5.3. The effect of vibration frequency on operating performance

According to section 3.1 parameter taking value selected A is 9 mm, V is 0.3 m/s, digging depth is 500 mm, vibration frequency f is 6.67, 8.67, 10.67 Hz, design single-factor test to clarify the effect of vibration frequency on operating performance.

5.3.1. Effect of vibration frequency on traction resistance and driving torque

The test results are shown in **Figure 18**, where strong and weak cycles of F and T occur, and f is negatively correlated with F and T. When f is 6.67, 8.67 and 10.67 Hz, the average values of traction resistance $\bar{F}$ in A_T cycle are 1476.38, 955.06 and 891.39 N, and the maximum values of driving torque T_{max} are 106.07, 109.41 and 128.65 N·m respectively. The average values of traction resistance $\bar{F}$ in B_T cycle are 1866.38, 1719.55, and 1416.43 N, and the maximum values of driving torque T_{max} are 364.19, 329.90, and 315.28 N·m, respectively. When f increases from 6.67 Hz to 8.67 Hz, $\bar{F}$ has a small change in the B_T cycle and T_{max} has a large increment in the B_T cycle; when f increases from 8.67 Hz to 10.67 Hz, $\bar{F}$ has a large change in the B_T cycle and T_{max} has a large increment in the A_T cycle. In a comprehensive analysis, the change in $\bar{F}$ is large when f increases from 8.67 Hz to 10.67 Hz, and the change in T_{max} is more stable.

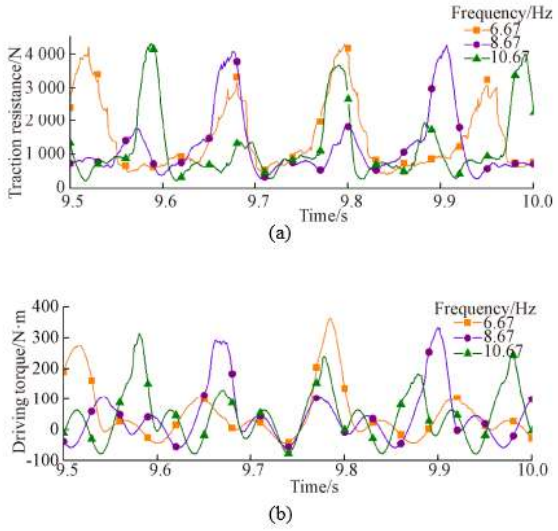

Figure 18. Effects of vibration frequency on traction resistance and driving torque, **(a)**. Effects of frequency on traction; **(b)**. Effects of frequency on driving torque.

5.3.2. Vibration frequency on the impact of throwing ability

The maximum value of the separation spacing occurs at the moment of termination of the strong cycle (B_T) cutting stroke, and the separation spacing H is obtained for seven characteristic points such as E_{W0} at f of 6.67, 8.67, and 10.67 Hz according to the method in Section 5.1.2, as shown in **Figure 19**.

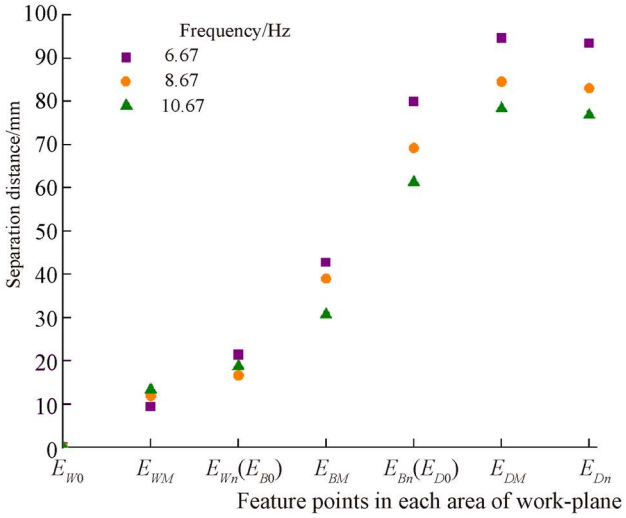

Figure 19. Effects of frequency on separation distance.

As can be seen from **Figure 19**, the vibration frequency f is negatively correlated with the separation distance H. The maximum value of H_{max} occurs at the middle point of the separation zone E_{DM} (due to the influence of soil viscoplasticity, the soil at the termination point of the separation zone E_{Dn} has fallen back to a certain height from the highest point). f is 6.67, 8.67 and 10.67 Hz, H_{max} is 94.67, 84.62 and 78.43 mm respectively. B_T There is a large amount of change in H_{max} when f increases from 6.67 Hz to 10.67 Hz during the cycle.

5.3.3. Effect of vibration frequency on separation capacity

The soil quality of each quality monitoring area of the working face within 2.5 s of stable operation duration was counted, and the separation percentage C of each area of the working face at f of 6.67, 8.67, and 10.67 Hz was obtained according to the method in section 5.1.2. as shown in **Table 3**.

Table 3. Separation proportion in each working area under different vibration frequency (%).

Vibration frequency/Hz	Monitoring area 1, 2 $C_1 + C_2$	Monitoring area 3, 4 $C_3 + C_4$	Monitoring area 5 C_5
6.67	63.9	30.06	6.04
8.67	64.29	31.3	4.41
10.67	64.29	33.4	2.31

From the analysis in **Table 3**, it can be seen that when f is 6.67, 8.67 and 10.67 Hz, the separation ratio $C_1 + C_2$ in the dispersion zone remains at about 64%, and the overall change of separation ratio $C_3 + C_4$ in the separation zone is not obvious, which is influenced by soil viscoplasticity, and the vibration frequency f has less influence on the separation ratio C. As f increases, it can promote soil fragmentation and dispersion flow to a certain extent, which is conducive to soil permeability fence and thus reduce the amount of unseparated soil.

5.4. Forward speed on operational performance

According to section 3.1 parameter taking values selected A is 9 mm, f is 8.67 Hz, digging depth is 500 mm, V is 0.2, 0.3, 0.4 m/s, design a single-factor test to clarify the effect of forward speed on operational performance.

5.4.1. Impact of forward speed on traction resistance and driving torque

The test results are shown in **Figure 20**. The traction resistance F and driving torque T increase with obvious strong and weak cycle phenomenon, V is positively correlated with F and T, and negatively correlated with H.

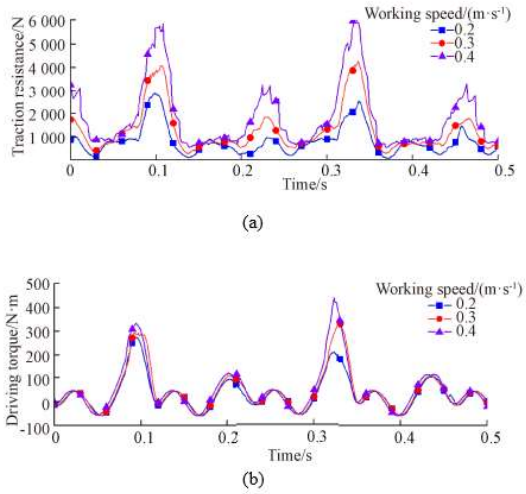

Figure 20. Effects of forward speed on traction resistance and drive torque, **(a)**. Effects of working speed on traction; **(b)**. Effects of working speed on driving torque.

When V is 0.2, 0.3 and 0.4 m/s, the mean values of traction resistance $\bar{F}$ are 655.85, 934.56 and 1425.65 N and the maximum values of driving torque T_{max} are 92.19, 106.81 and 119.79 N·m for A_T cycle, respectively. The mean values of B_T cycle traction resistance $\bar{F}$ are 1429.43, 1719.55, 2110.48 N, and the maximum values of driving torque T_{max} are 241.27, 299.07, 387.78 N·m. When V increases from 0.2 m/s to 0.3 m/s, $\bar{F}$ has a large change in the B_T cycle, and T_{max} has a small increment in the A_T cycle and a large increment in the B_T cycle; when V increases from 0.3 m/s to 0.4 m/s, both $\bar{F}$ and T_{max} have a large increment in the B_T cycle. The overall analysis shows that the changes of $\bar{F}$ and T_{max} are more stable when V increases from 0.2 m/s to 0.3 m/s.

5.4.2. Impact of forward speed on throwing ability

The maximum value of the separation distance occurs at the end moment of the cutting stroke of the B_T cycle, and the separation distance H is obtained for seven characteristic points such as E_{W0} when V is 0.2, 0.3 and 0.4 m/s according to the method in section 5.1.2, as shown in **Figure 21**.

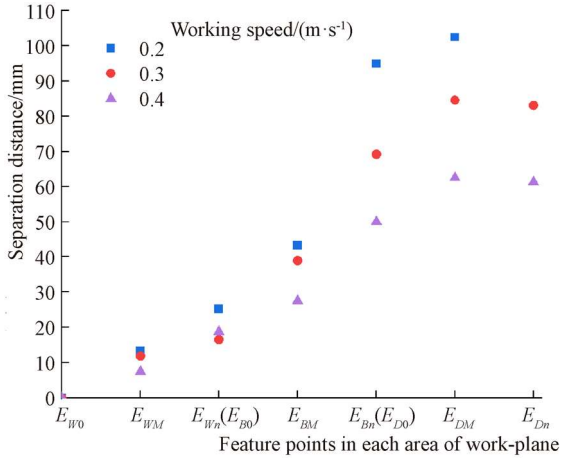

Figure 21. Effects of forward velocity on separation distance.

As can be seen from **Figure 21**, H is negatively correlated with *V*. The maximum value of H_{max} occurs at the middle point of the separation zone, E_{DM} (affected by soil viscoplasticity, the soil has fallen back from the highest point at the termination point of the separation zone, E_{Dn}). H_{max} was 102.5, 84.62, and 62.5 mm for *V* 0.2, 0.3, and 0.4 m/s, respectively. The strongest throwing ability was found at *V* 0.2 m/s, and the soil at the front of E_{Dn} was completely permeable to the fence and bare fence bars were observed, so no H value was recorded at E_{Dn}.

5.4.3. Impact of forward speed on separation capacity

The soil quality of each quality monitoring area of the working face during the stable operation duration of 2.5 s was counted, and the separation ratio *C* was obtained for each area of the working face when *V* was 0.2, 0.3, and 0.4 m/s according to the method in section 5.1.2. As shown in **Table 4**.

Table 4. Separation proportion in each working area under different working speed (%).

Working speed/(ms^{-1})	Monitoring area 1, 2 $C_1 + C_2$	Monitoring area 3, 4 $C_3 + C_4$	Monitoring area 5 C_5
0.2	64.18	35.82	0.00
0.3	64.59	31.00	4.41
0.4	49.17	25.91	24.92

As can be seen from the analysis in **Table 4**, when V increases from 0.2 m/s to 0.3 m/s, there is no significant change in the dispersed region $C_1 + C_2$, and the undetached region C_5 increases from 0 to 4.41%; when *V* increases from 0.3 m/s to 0.4 m/s, the dispersed region $C_1 + C_2$ decreases sharply, the detached region $C_3 + C_4$ decreases from 31% to 25.91%, and the undetached region C_5 surges from 4.41% to 24.92%. A comprehensive analysis shows that *V* of 0.3 m/s has a high soil separation efficiency.

6. Field trials

6.1. Test conditions and methods

The authors' team developed and designed a 4GSZ–145 licorice harvester (operating width 1450 mm) based on a single-swing shovel-grid harvesting device, and conducted field trials in Yanchi County, Wuzhong City, Ningxia Province, in October 2021. The test plot was about 75 m long and 60 m wide, with gray calcium soil, soil moisture content of about 7.76%, and soil firmness of 2150–3208 kPa; the licorice variety was Ural licorice. Work tractor for JD6B–1404 (output shaft speed 1000 r/min, power output power ≥ 87.6 kW), tractor for JD6B–1204 (traction power ≥ 39 kW); other test instruments and equipment including 0CS-Y–5t

tensiometer, HP-DS8X25 dynamic signal tester, XH60130 type collector ring, shovel electronic scale, stopwatch, steel plate ruler, woven bag, label, etc.

Work tractor suspension licorice harvester, through the three-point suspension device to control the harvester operating depth, its power output shaft connected to the universal joint to provide excitation force for the harvester; operation, the tractor gear in a neutral position, by the tractor dragged forward through the tow rope, the test process as shown in **Figure 22**. According to the parameters taken in section 3.1 and site conditions, the test parameters A is 9 mm, f is 9.4 Hz, V is 0.32 m/s; test measurement area 3, each measurement area length 10 m, traction resistance, driving torque, digging depth, harvesting net rate and other indicators are obtained using the following methods.

Figure 22. Field experiment of licorice harvest, **(a)**. Experimental process; **(b)**. Throwing effects of oscillating slat shovel.

Traction resistance (F): read directly from the tensiometer display, each measurement area to record 10 data to calculate the average value, traction resistance F calculated by Equation (19).

$$F = \frac{\sum_{i=1}^{10} F_{Zi}}{10} - F_K \tag{19}$$

where F_{Zi} is the ith tractive force value during harvesting operation, kN; F_K is the no-load tractive force during unearthed operation, kN.

Driving torque (T): It is measured by the principle of full-bridge strain measurement. A set of full-bridge strain gauges is arranged in the universal joint, and the strain bridge deformation information is transmitted to the dynamic signal tester through the current collector to complete data acquisition and analysis. The waveform intercepts the valid data interval and calculates the average deformation value in this area. The driving torque T is calculated by the calibration Equation (20).

$$T = 0.008 \times \overline{\varepsilon} - 2.955 \tag{20}$$

where $\overline{\varepsilon}$ is the mean value of the effective form variable, μm .

Excavation depth ($\overline{D}$): 5 measurement points were selected equidistantly within each measurement area, and the vertical distance from the maximum excavation depth to the surface of the last plowed land was measured by using a steel plate ruler and recorded as the excavation depth. The average excavation depth $\overline{D}$ is calculated by Equation (21).

$$\overline{D} = \frac{\sum_{i=1}^{5} D_i}{5} \tag{21}$$

where D_i is the excavation depth of the i-th measurement point, mm.

Net harvest rate (η): The licorice that can be directly seen on the surface (effective harvesting licorice) was picked up and weighed in each measurement area, and recorded as m_1; then the soil was dug up with a shovel to find the licorice left in the soil (missed digging licorice) and weighed in, and recorded as m_2. The net rate of licorice harvesting can be calculated by Equation (22).

$$\eta = \frac{m_1}{m_1 + m_2} \times 100\% \tag{22}$$

where m_1 is the effective harvest mass, g; m_2 is the missed digging mass, g.

6.2. Experimental results and analysis

The results of the field tests are shown in **Table 5**. The average traction resistance of the licorice harvester was 32.17 kN, the average driving torque was 802.02 N·m, the average digging depth was 468 mm, and the average net harvesting rate was 96.42%. Due to the limitation of the test conditions, the accurate soil separation ratio data of each functional area of the shovel grate working surface could not be obtained. The test results show that: the process of licorice harvesting is smooth and orderly, the monopod grate can effectively throw the soil, the height of the marked licorice and soil pieces thrown away from the grate gradually increases during the backward movement, and the soil pieces breaking up intensifies, the gradual throwing effect of the monopod grate is obvious, the root and soil separation performance is good, and the working principle of the monopod grate harvesting device is scientific and feasible.

Table 5. Field experimental results.

Measuring areas	Traction resistance/kN	Driving torque/ N·m	Excavation depth/mm	Collection rate/%
1	32.71	802.68	475	97.44
2	31.64	779.21	467	97.22
3	32.16	824.16	462	94.59
Mean values	32.17	802.02	468	96.42

7. Conclusion

(1) The throwing coefficient is defined, and the analytical equation of the throwing coefficient is established. The throwing coefficient at each point of the working surface varies sinusoidally and can effectively throw the soil when the throwing coefficient is greater than 0. The throwing coefficient is positively related to the amplitude and vibration frequency and gradually increases with the increase in working length.

(2) Simulation test results show that: affected by the throwing characteristics of the working surface and soil viscoplasticity, the traction resistance and driving torque show obvious strong and weak cycles, and the mutual force between the shovel fence and soil is larger in the strong cycle; the maximum value of the separation distance is generated at the middle point of the separation zone at the end of the cutting stroke of the strong cycle; the separation ratio of the dispersion zone changes less under each working condition.

(3) Amplitude A is negatively correlated with traction resistance F and positively correlated with driving torque T and separation distance H; vibration frequency f is negatively correlated with F, T, and H; forward speed V is positively correlated with F and T and negatively correlated with H; A and f have less influence on the separation ratio C. The amount of soil increases with V, thus leading to poorer separation performance of the single pendulum shovel grid throw.

(4) The field test results show that: the average traction resistance of the licorice harvester is 32.17 kN, the average driving torque is 802.02 m, the average digging depth is 468 mm, the average harvesting net rate

is 96.42%, the operation process is smooth and orderly, the gradual throwing effect is obvious, the root and stem soil separation performance is good, and the single swing shovel fence has good potential in root and stem crops, especially deep root and stem crops. It has good application potential in the field of energy-saving and efficient harvesting of root crops, especially deep root crops.

Conflict of interest

The authors declare no conflict of interest.

References

1. Yang R, Yang H, Shang S, et al. Design and test of vertical annular separation and conveying device for potato combine harvester (Chinese). *Transactions of the Chinese Society of Agricultural Engineering* 2018, 34(3): 10–18.
2. Zhao Q. Research status and development prospect of potato harvesting machinery at home and abroad (Chinese). *Agricultural Engineering* 2020, 10(6): 7–10.
3. Yang R, Wang Z, Shang S, et al. Design and test of rice bale coating device for peanut joint harvest silage machine (Chinese). *Transactions of the Chinese Society for Agricultural Machinery* 2020, 51(8): 109–117.
4. Luo Q, Ning H, Liu Y, He M. Analysis and evaluation of the current status of rooibos and licorice resources in Xinjiang (Chinese). *Protection Forest Science and Technology* 2019; 5: 13–16.
5. You Z, Hu Z, Wu H, et al. The design and test of 1MCDS–100 A shovel sieve residual film reclaimer (Chinese). *Transactions of the Chinese Society of Agricultural Engineering* 2017; 33(9): 10–18.
6. Zhang R, Sun W, Wu J, et al. The design and research of shovel-screen excitation potato excavator (Chinese). *Research of Agricultural Modernization* 2015; 36(5): 916–920.
7. Zhang Z, Wang Y, Li H, et al. Design and test of hydraulic control crawler self-propelled greenhouse panax notoginseng harvester (Chinese). *Transactions of the Chinese Society for Agricultural Machinery* 2021; 52(6): 127–135, 158.
8. Wei Z, Li H, Su G, et al. The research and development of buffer sieve potato harvester (Chinese). *Transactions of the Chinese Society of Agricultural Engineering* 2019; 35(8): 1–11.
9. Zhang Y, Ou Z, Cui Z, et al. Design and experimental analysis of double roller combined pineapple leaf crushing and returning machine (Chinese). *Journal of Agricultural Science and Technology* 2017; 19(7): 78–86.
10. Yang F, Yang Y, Li W, et al. Design and test of vibration excavation crushing device for hanging yam harvester (Chinese). *Transactions of the Chinese Society for Agricultural Machinery* 2020; 51(6): 104–111.
11. Kim YS, Siddique AA, Kim WS, et al. DEM simulation for draft force prediction of moldboard plow according to the tillage depth in cohesive soil. *Computers and Electronics in Agriculture* 2021; 189: 106368. doi: 10.1016/j.compag.2021.106368
12. Deng G, Huang Y, Zheng S, et al. Improved design and test of vibration chain cassava harvester (Chinese). *Modern Agricultural Equipment* 2018; 3: 35–39.
13. Lipiec J, Czyż EA, Dexter AR, et al. Effects of soil deformation on clay dispersion in loess soil. *Soil and Tillage Research* 2018; 184: 203–206. doi: 10.1016/j.still.2018.08.005
14. Yang R, Yang H, Shang S, et al. The design and test of roller push potato harvester (Chinese). *Transactions of the Chinese Society for Agricultural Machinery* 2016; 47(7): 119–126.
15. Hou J, Chen Y, Li Y, et al. Development of quantitative self-propelled onion combine harvester (Chinese). *Transactions of the Chinese Society of Agricultural Engineering* 2020; 36(7): 22–33.
16. Yang Y, Liao Y, Wang T, et al. Design of self-propelled cassava harvester (Chinese). *Journal of Agricultural Mechanization Research* 2016; 38(4): 99–102+106.
17. Lyu J, Sun H, Dui H, et al. Improved design and test of separation and transportation device for potato excavators in sticky soil (Chinese). *Transactions of the Chinese Society for Agricultural Machinery* 2017; 48(11): 146–155.
18. Xie S, Wang C, Deng W, et al. Mechanism analysis and parameter optimization test of swing separation sieve potato soil separation (Chinese). *Transactions of the Chinese Society for Agricultural Machinery* 2017; 48(11): 156–164.
19. Wei Z, Su G, Li X, et al. Optimization and test of wave screen surface parameters of potato harvester based on discrete element (Chinese). *Transactions of the Chinese Society for Agricultural Machinery* 2020; 51(10): 109–122.
20. Zhang Chao. *Design and Experimental Study of Vibrating Grid Licorice Harvester for Combined Excavation* (Chinese) [Master's thesis]. China Agricultural University; 2021.
21. Sun Y, Dong X, Song J, et al. Operation parameters optimization of vibration subsoiling test bench (Chinese). *Transactions of the Chinese Society of Agricultural Engineering* 2016; 32(24): 43–49.
22. Dong X, Song J, Wang J, et al. The motion characteristics analysis and vibration frequency optimization of

grassland vibration subsoiler (Chinese). *Transactions of the Chinese Society of Agricultural Engineering* 2012; 28(12): 44–49.
23. Sun Y, Dong X, Song J, et al. The self-balancing performance and simulation analysis of multiple vibration subsoilers of vibration subsoilers (Chinese). *Transactions of the Chinese Society of Agricultural Engineering* 2018; 34(4): 92–99.
24. Liu W, He J, Li H, et al. Design and test of double side deep fertilization device for potato micro potato planting machine (Chinese). *Transactions of the Chinese Society for Agricultural Machinery* 2020; 51(1): 56–65.
25. Zhao S, Liu H, Hou L, et al. Development of no-tillage and deep-fertilization sectional corn sowing trencher based on discrete element method (Chinese). *Transactions of the Chinese Society of Agricultural Engineering* 2021; 37(13): 1–10.
26. Yu W, Yang R, Shang S, et al. The design and test of shovel-screen combined peanut segmental harvester (Chinese). *Journal of Agricultural Mechanization Research* 2016; 38(6): 163–166+171.
27. Cheng C, Fu J, Chen Z, Reng L. Vibration parameters of the vibrating screen of the harvester affect the adhesion characteristics of different humidity extracts (Chinese). *Transactions of the Chinese Society of Agricultural Engineering* 2019; 35(8): 29–36.
28. Thakur SC, Morrissey JP, Sun J, et al. Micromechanical analysis of cohesive granular materials using the discrete element method with an adhesive elasto-plastic contact model. *Granular Matter* 2014; 16(3): 383–400. doi: 10.1007/s10035-014-0506-4
29. Xie F, Wu Z, Wang X, et al. The calibration of soil discrete element parameters based on unconfined compressive strength test (Chinese). *Transactions of the Chinese Society of Agricultural Engineering* 2020; 36(13): 39–47.
30. Zhang R, Han D, Ji Q, et al. Study on calibration method of sandy soil parameters in discrete element simulation (Chinese). *Transactions of the Chinese Society for Agricultural Machinery* 2017; 48(3): 49–56.
31. Wang X, Hu H, Wang Q, et al. The calibration method of soil model parameters based on discrete element (Chinese). *Transactions of the Chinese Society for Agricultural Machinery* 2017; 48(12): 78–85.